Filtered Geometry Modelling for Fan-intake interaction Based on the Immersed Boundary Method

Yunfei Ma, Paul Tucker

Department of Engineering, University of Cambridge, UK, CB2 1PZ, ym324@cam.ac.uk

ABSTRACT

The Immersed Boundary Method has showed promising applicability for a range of fundamental flows and turbulence simulations. However, to the authors' knowledge, flows in coupled components or coupled physics scenarios, such as rotor-stator interaction, fan-intake interaction, aeroelastics, aeroacoustics, etc. are still rarely investigated using high-fidelity method. Due to its demanding computational costs, the complexity of geometry meshing process and moving boundaries limit the investigation of flows in this environment. Hence, high-fidelity simulations with an acceptable geometry modelling strategy may tackle this issue and provide more insightful understanding. There is a hierarchy of geometry modelling methods which includes the conventional Direct Mesh Resolved (DMR) method, the Immersed Boundary Method (IBM) and the IBM with Smeared Geometry (IBMsg). The present research proposed an IBM with filtered geometry (IBMfg). This method can include more realistic flow physics within each blade passages without smearing the blade cascade. It is applied to study fan-intake interaction and the focuses are on the inlet distortion transport through blade passages.

KEYWORDS

Intake distortion, Geometry Modelling, Mixed-fidelity

NOMENCLATURE

a_n coefficients of Fourier series
$\boldsymbol{f}$ force
F_d force density
H height of the beam
$H(x)$ Heaviside function
N number of blade
K viscosity coefficient of parallel force
k coefficient for viscosity distribution
R_b blade length
$\boldsymbol{n}$ normal vector to the blade camber line
$\boldsymbol{p}$ parallel vector to the blade camber line
$\boldsymbol{u}$ velocity
π_t total pressure ratio
V solid velocity
u flow velocity
u_{ref} reference velocity
s fraction of blade span
$\boldsymbol{x}_0$ body/surface coordinate
$\boldsymbol{X}$ blade configuration
δ Dirac function
δ_b blade thickness
PI Porportional-Integral
CFD Computational Fluids Dynamics
DMR Directly Mesh Resolved
RANS Reynolds Averaged Navier-Stokes
URANS Unsteady Reynolds Averaged Navier-Stokes
LES Large Eddy Simulation
IBM Immerse Boundary Method
IBMsg Immersed Boundary Method with Smeared Geometry
IBMfg Immersed Boundary Method with Filtered Geometry

INTRODUCTION

The present industrial CFD application tends to rely heavily on computer performance in order to simulate and understand the turbulence within complex and challenging flows. Due to the potential failure of RANS-based turbulence models for separated or vortical flows (Liu et al.; 2008, 2016), the turbulence in such flows needs to be well resolved by high-fidelity simulations rather than modelled by RANS. The high-fidelity eddy resolving simulations, such as DNS and LES, and hybrid RANS–LES have demonstrated very accurate and promising results (Spalart; 2000; Liu et al.; 2017). However, the mesh resolutions are very demanding. An alternative solution could be hybrid RANS–LES (Haase et al.; 2009). Whether RANS or LES is applied depends on non-dimensional wall-normal distance. This could be feasible for simple computational domains. However, geometries in turbomachines could be extremely complex. They contains a number of rotational and static blade passages, and sometimes very complicated test probes or a distortion generator. Conventionally, these components are meshed using CAD tools and then deformed into computational demain in a CFD solver. The complexity can significantly increase the meshing and computing time, which is still not acceptable. Therefore, an alternative computer method that can avoid these drawbacks while preserving numerical accuracy is definitely a huge progress for the industrial high-fidelity CFD application.

The Immersed Boundary Method (IBM) provides a potential way to improve the efficiency for flow simulations in turbomachines. It replaces the surfaces of complex geometric configurations by a distribution of 'force'. Hence, the boundaries of those components are immersed within flows and the original complicated mesh can be substituted by a Cartesian-like mesh. Accordingly, the meshing process and deformation can be considerably simplified; as a result, the mesh size and computing time are reduced.

The fundamental idea of replacing boundaries by forces was firstly introduced by Sirovich (Sirovich; 1967). When solving linearised initial and boundary value problems, Sirovich converted the boundaries of original computation domains to source terms (momentum and energy rates in his case) in governing equations. Hence, the problem became initial value problem in an unbounded domain. Applications of the IBM were conducted for a range of studies of 2D flows around a circular cylinder and 3D channel flows (Basdevant and Sadourny; 1984; Goldstein et al.; 1993). Simulations for turbulent flows around complex geometries were also carried out by Iaccarino and Verzicco (Iaccarino and Verzicco; 2003), Mittal and Iaccarino (Mittal and Iaccarino; 2005). These include steady and unsteady flows at Reynolds numbers ranging from 10 to 10^6. However, for turbomachines, the internal geometries, such as blade passages are usually very complicated. Hence, resolving the boundary layers on blade surfaces requires very fine mesh and numerous computing resources. In this scenario, the IBM does not show many advantages compared to the conventional blade meshing method. To deal with this issue, Cao et al. (Cao et al.; 2016) have proposed a specific simplified version, the Immersed Boundary Method with smeared geometry (IBMsg). The smeared geometry means the geometric features are averaged in periodic direction, that is, circumferential direction for turbomachines. This assumes an infinite number of blades in a row of rotors and stators. Hence, the force of blades are distributed into each computation cell within blade region. Due to this fact, the forces are also known as Body Forces. Since no individual blade passage is resolved, the computational cost can be significantly reduced.

The IBMsg method indeed performs well when variations in circumferential direction are ignored. However, when considering full 3D simulations, it is not applicable due to the smeared geometry or infinite blade assumption. Although some research (Defoe et al.; 2009; Defoe and Spakovszky; 2013) proposed body force perturbations to generate blade-to-blade variations, the

model still relies on the prerequisite data from RANS of a single rotor passage and a subsequent reconstruction process. Hence, to reflect more realistic flow physics in three dimensions while keeping a lower computing cost, we propose a IBM with filtered geometry (IBMfg). To the authors' knowledge, little work has been done to model rotor or stator with actual finite blades, this paper addresses this issue and develop a proper force modelling method to simulate flow features for finite blade passages. Distribution of flow variables are compared against experiment data, mesh resolved case and IBMsg case.

METHODOLOGY

The present research employs an indirect force model proposed by Mohd-Yusof (Mohd-Yusof; 1997). This method does not rely on any empirical coefficients in feedback forcing, and hence does not have limitations from computation stability. We apply it to replace boundaries of rotor and stator blades. The blade forces are decomposed in normal and parallel directions to the blade camber line. When supplemented with the blade force $\boldsymbol{f}_b$, Mohd-Yusof's model gives

$$f_n^{l+1/2} = -RHS^l + \frac{V_n^{l+1} - u_n^l}{\partial t}, \tag{1}$$

where l is the time level, $1/2$ denotes the process for force configuration, and RHS^l contains convective and viscous terms and the pressure gradient from the Navier–Stokes equation. When flows fit a given blade angle, then ideally $u_n^{l+1} = V_n^{l+1}$ within immersed blade region. The velocity $V_n^{l+1} = \boldsymbol{r} \times \boldsymbol{\Omega} \cdot \boldsymbol{n}_0$ for the rotational rotor blades and zero for the stator.This force will then turns flows towards the desired angle directly without any dynamical process as the PI controller does. At every time step, this is determined only by fan blade geometries regardless of flow frequencies and constants that feedback forcing relies on. Consequently, the time step can be increased and CPU time can be significantly reduced.

According to Watson's research (Watson et al.; 2017), the parallel force characterises the loss of flows passing through blade passages and is modelled as,

$$f_p = -(4s^2 + 1)k\rho \boldsymbol{u}_{rel}^2, \tag{2}$$

where s is the fraction of span and the coefficient k is a calibration constant set to 0.2 [1]. Although the use of loss model cannot provide too much detail within blade passages, it is still able to provide a relatively accurate 'boundary' for regions in the upstream or downstream. For the studies of the region between interactive components, such as fan-intake research, this method can provide an economical solution while preserving accuracy.

The distribution of forces is the core for blade modelling. The forces obtained from Eq.1 and 2 can be regarded as a 'force density $\boldsymbol{F}_d$' defined in Peskin's (Peskin; 2002) theory. As a consequence, the blade can enforce the flows through the Dirac function δ as,

$$\boldsymbol{f}(\boldsymbol{x}, t) = \int \boldsymbol{F}_d \delta \left(\boldsymbol{x} - \boldsymbol{X}(\boldsymbol{x}_0, t)\right) \mathrm{d}\boldsymbol{x}_0, \tag{3}$$

where $\boldsymbol{X}(\boldsymbol{x}_0, t)$ is the configuration of blade immersed in the flow. The Dirac function is defined as

$$\delta \left(\boldsymbol{x} - \boldsymbol{X}(\boldsymbol{x}_0, t)\right) = \begin{cases} \infty, & \boldsymbol{x} = \boldsymbol{X}(\boldsymbol{x}_0, t). \\ 0, & \boldsymbol{x} \neq \boldsymbol{X}(\boldsymbol{x}_0, t). \end{cases} \tag{4}$$

[1] calibrated by experimental data and/or resolved blade data at design points.

and

$$\int_V \delta\left(\boldsymbol{x}-\boldsymbol{X}(\boldsymbol{x}_0,t)\right)\mathrm{d}\boldsymbol{x}=1, \tag{5}$$

where 'V' denotes the whole computation region. In practice, an analytical distribution function is applied to approximate the Dirac Function. Considering the periodic features of fan blades in circumferential direction, a square wave function is chosen. Thus the normal and parallel forces can be configured as

$$\mathcal{F}(\boldsymbol{x},t)=H(R_b-r)\sum_{n=0}^{\infty}a_n cos(\theta+\theta_0+\Omega t), \tag{6}$$

and

$$a_n=\frac{2}{n\pi}sin\left(\frac{nN\delta_b}{2r}\right). \tag{7}$$

In this formula, $H(R_b-r)$ is the Heaviside step function, r is radial coordinate and R_b is the blade length in spanwise direction. This considers the rotor blade clearance due to the definition

$$H(R_b-r)=\begin{cases}1, & r<R_b.\\ 0, & r\geqslant R_b.\end{cases} \tag{8}$$

In the series part, θ is circumferential direction in cylindrical coordinate, θ_0 is the circumferential location of blade camber line, N is the number of fan blades, Ω is the rotational speed of fan, and δ_b is the thickness of blade. It should be noted that θ_0 and δ_b are also functions of space determined by blade location and shape respectively, meaning that the blade profile has been considered. Thus, the blade forces can be expressed as

$$\boldsymbol{f}_b(\boldsymbol{x},t)=(f_n\boldsymbol{n_0}+f_p\boldsymbol{p_0})\mathcal{F}(\boldsymbol{x},t), \tag{9}$$

where $\boldsymbol{n_0}$ and $\boldsymbol{p_0}$ are the unit vectors in the directions normal and parallel to blade camber line.

Essentially, this form of force is distributed within the blade region but the geometry is actually still smeared according to the blade camber line. This means that on the blade surface, the flow may not follow the curves on either pressure surface or suction surface, but the camber line. Hence, the force outside a blade is filtered out. This is where the name IBMfg comes from. Indeed, due to the coarse resolution of the boundary layer on blade surfaces, this approximation may not accurately predict the transition or viscosity-induced separation near the blade trailing edge. However, since the compressor blades are usually very thin and the aim of the research is to generate suitable boundary conditions for the upstream or downstream flows, its disadvantages could be neglected.

Finally, the IBMfg blades can be implemented in the compressible Navier–Stokes equations as

$$\frac{\partial}{\partial t}\int_\Omega \mathbf{q}d\Omega+\oint_A \mathbf{G}\cdot d\boldsymbol{A}=\int_\Omega \mathbf{F}d\Omega+\int_V \mathbf{S}dV, \tag{10}$$

where

$$\mathbf{q}=\begin{pmatrix}\rho\\ \rho v_x\\ \rho v_y\\ \rho v_z\\ \rho E\end{pmatrix},\mathbf{G}=\begin{pmatrix}\rho\boldsymbol{v}\\ \rho v_x\boldsymbol{v}+p\boldsymbol{n}_x\\ \rho v_y\boldsymbol{v}+p\boldsymbol{n}_y\\ \rho v_z\boldsymbol{v}+p\boldsymbol{n}_z\\ \rho H_e\boldsymbol{v}\end{pmatrix},\mathbf{F}=\begin{pmatrix}0\\ f_{b,x}\\ f_{b,y}\\ f_{b,z}\\ \boldsymbol{f_b}\cdot\boldsymbol{v}\end{pmatrix}, \tag{11}$$

and $\mathbf{S}$ contains viscous terms.

Table 1: Key parameters of the Darmstadt Transonic Compressor, (Wartzek et al.; 2016)

Design mass flow	16 kg/s
Design speed	20,000 rpm
Outer diameter	0.38 m
Hub-to-tip-ratio	0.51
Rotor/stator blades	16/29

Table 2: Costs for IBMfg(sg) and DMR cases

Methods	IBMfg(sg)	DMR
Mesh size	12.4M	61.4M
Mixing plane	No	Required
Mesh type	Orthogonal	C type
Computing time*	9.8h	122h

* 480CPUs, per revolution.

NUMERICAL FRAMEWORK

The IBMfg are tested on a full-annulus Darmstadt Transonic Rotor (Bitter et al.; 2015; Wartzek et al.; 2016, 2015) for exploring main flow features. The key parameters of the Darmstadt Rotor is listed in Table 1 and the sketch of the flow domain can be found in Fig.1. The distortion generator is the same as Wartzek's (Wartzek et al.; 2016) test rig, which covers $120°$ in circumferential direction. The case is run at 100% and 65% rotational speed (RS) using RANS with $k-\omega$ model. Inlet boundary conditions are $p_0 = 101325$Pa and $T_0 = 288.15$K, whereas the outlet applies fixed static pressures with radial equilibrium conditions. In addition, the data from an IBMsg case, a DMR (distortion generator, rotor and stator) case and the experiment (Wartzek et al.; 2016) are also compared.

Both the IBMfg and IBMsg case use the same mesh with 12.4M nodes, compared to the DMR case with 61.4M nodes. Table 2 compares the costs for both cases and also notes their computing time, showing that the time for running an IBMfg case could be saved by almost 90%. The sketch of the mesh is depicted in Fig.2. It should be noted that Fig.2a just depicts a coarsened mesh for the reveal of blade locations. The data are compared and validated at three cross-sections at $S1 = 3.5$, $S2 = 8.5$ and $S3 = 12$ (Fig.1).

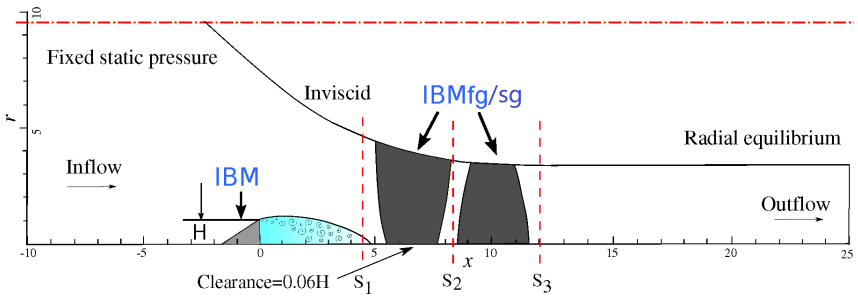

Figure 1: Sketch of a full-annulus case: Boundary conditions and monitored planes

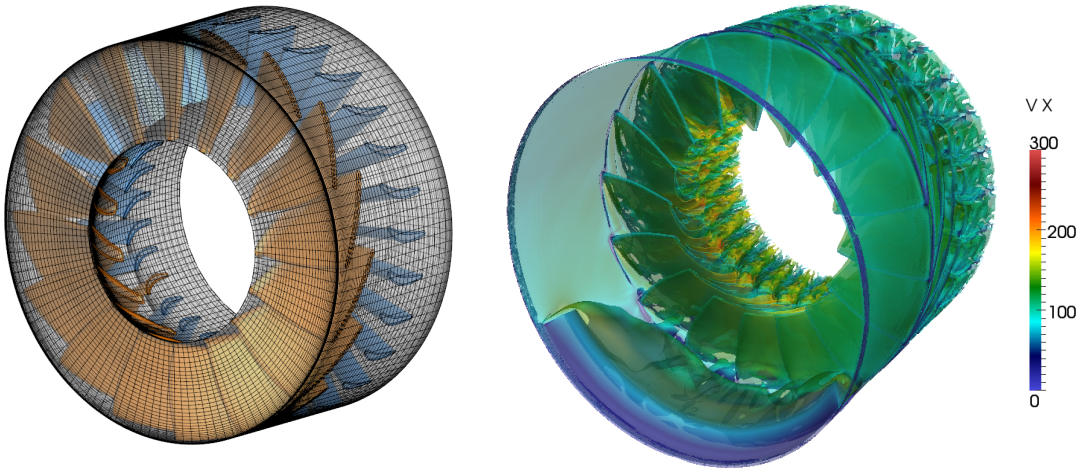

(a) Sketch of IBMfg mesh for blade region (coarsened for the view)

(b) Iso-surface of Q-criterion 5×10^6, coloured by axial velocity (m/s)

Figure 2: Test case: (a) IBMfg/IBMsg mesh (b) Q-criterion iso-surface

RESULTS

We examine the effectiveness of IBMfg compared to the IBMsg, DMR case and experiment. The test case is run at the peak efficiency point of 10.6kg/s with 65% rotational speed. Figure 2b depicts the iso-surface of Q-criterion at 5×10^6 for the full-annulus case. The view is taken from the inlet, and it can be seen that the distortion generator creates substantial separated flows in front of the rotor. The rotor with 16 blades can be clearly represented using IBM. Both the blade configuration and its thickness are well modelled.

Contours

This section compares the flow distributions between the DMR case and IBMfg case and depicts the interaction between the blades and separation bubble downstream the distortion generator. The contours are extracted near the casing within the blade clearance. In general, the IBMfg case is able to capture very similar flow features compared to the DMR case.

Figure 3a depicts the static pressure distribution with a distortion generator placed at the centre in the upstream. The pressure rise across the rotor blade and its intermittent pressure wave towards the upstream are well captured. The pressure loss ($p < 1.0$, depicted in blue) around the blade leading edge is also correctly represented. Evidently, the separated flows from the distortion generator can impact the region around fan leading edge, but this impact can be finally suppressed within the rotor.

The distribution of the Mach number shown in Fig.3b (in the absolute frame) reveals the impact of the separation on the blade tip. The flow within the distortion region is strongly accelerated in both cases. This is because, when the separation enters the blade passage, it reduces the static pressure on the pressure surface and hence increases the pressure difference across a blade. Consequently, this pressure difference accelerates the flow within the tip clearance and thus the magnitude of the Mach number increases.

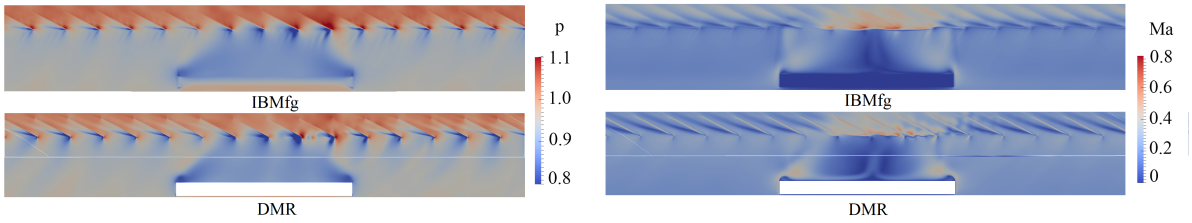

(a) Static pressure (referenced by $p_0 = 101325Pa$) (b) Mach number

Figure 3: Distribution of (a) static pressure and (b) Mach number near casing (within tip clearance)

Axial locations

Figure 4a-4c quantitatively compare the distribution of total pressure ratio at some axial locations for cases at design point with 100% and 65% rotational speed respectively. These cases are from the URANS with direct mesh resolved (DMR), RANS with IBMsg, URANS with IBMfg, and also experimental results. The data are extracted and averaged by area at: rotor inlet $S1$, rotor exit $S2$ and stator exit $S3$.

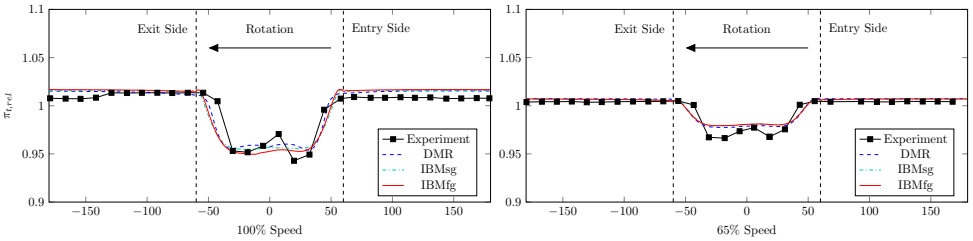

(a) Rotor inlet

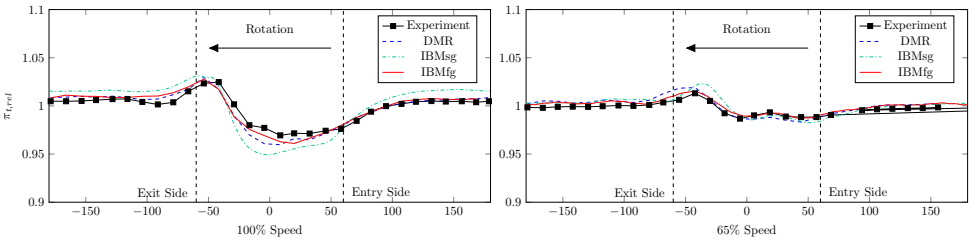

(b) Rotor outlet

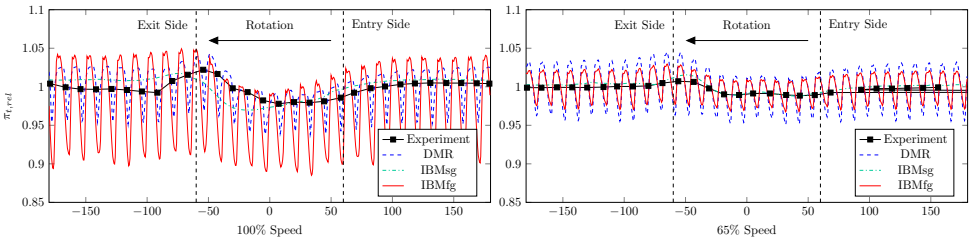

(c) Stator outlet

Figure 4: Total pressure distribution at three axial locations, averaged by area:(a) Rotor inlet, (b) Rotor outlet, (c) Stator outlet

In Fig.4a, the beam installation region is specified by the vertical dash lines, marking the entry side and exit side of the rotor. The total pressure ratio is lower within the region

$-60^\circ \leqslant \theta \leqslant 60^\circ$ where the distortion generator is installed in the upstream. The loss for the case with 100% Speed is higher, indicating stronger separation. The general trends among the three numerical simulations are very similar and also match the data obtained from Wartzek's experiment(Wartzek et al.; 2016). Interestingly, the experiment shows a W-shape in the center. This seems to be resulted from the corner vortices and the separation line shear layer at the two sides of the beam (Wartzek et al.; 2015). They intensify the total pressure loss at the edges of the separation region, but in the centre the loss still remains at the original level. However, this is not obvious in all the present numerial simulation for both cases. It is perhaps due to the fact that both URANS and RANS are not able to resolve such strong separation (Liu et al.; 2011; Tang et al.; 2018).

Figure 4b shows the distribution at the rotor outlet. Compared to the experiment and the DMR case, the case with modelled blades (both IBMfg and IBMsg) can successfully capture the distortion transport and its displacement towards entry side. The asymmetry of the total pressure distribution: the value at the exit side higher than the entry side, are also well predicted. Hence, it can be concluded that both geometry modelling methods can present an accurate distortion transport. However, it should be noted that the IBMsg case shows a certain extent of discrepancy at 100% speed within distortion region. This may be due to the assumption of infinite blades, which overestimates the pressure loss especially when the massflow rate or flow velocity is high. At the stator outlet in Figure 4c, both the IBMsg and IBMfg case can accurately reflect the transport of the distortion across the stator. However, as expected, the IBMsg case totally smears the wakes generated by the blades, whereas the IBMfg case is able to capture this feature. Compared to the DMR case, the IBMfg case still sees slight deviations in its magnitude, but this could be further resolved by refining the loss model.

Radial Locations

In radial direction, the data are obtained at 10%, 50% and 90% of the stator exit, corresponding to the hub, midspan and shroud locations, shown in Fig.5a-5c respectively.

At the hub (Fig.5a), both the distortion transport and blade wakes are well captured by the IBMfg, despite a small reduction in its magnitude within blade passages. It should be noticed that the experiment generally captures the maximum at all the circumferential locations; by contrast, the IBMsg seemingly averages the data within and outside blade wakes. Its discrepancy is higher for 100% speed because the wakes result in much lower total pressure due to overestimated loss.

In the midspan, the prediction from both IBMsg and IBMfg are much better and the wake loss is lower. The results are almost identical for 65% speed. This implies that the main flow features, including the distortion and wake loss, could be well captured by all the methods. Near the casing (Fig. 5c) because the blade work is the highest, the wake loss is the minimum and the discrepancy between IBMsg and other methods is also low.

These comparisons demonstrate that the IBMfg case can accurately predict both the distortion transport and blade wakes, whereas the IBMsg can roughly reflect the distribution of distortion but totally smears those wakes.

Blade Region

Within the rotor blade region, the IBMfg case also demonstrates a good result in terms of the static pressure at both pressure and suction surface of blades. By contrast, the IBMsg smears the variation in circumferential direction and only shows a straight line, and hence is not compared. Figure 6 depicts the distribution from three different radial locations extracted near the rotor

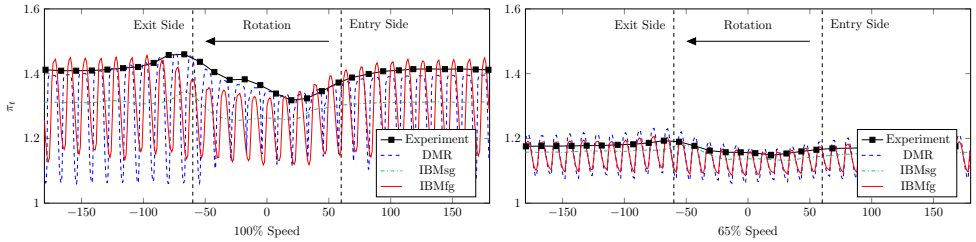

(a) Hub, 10% blade height

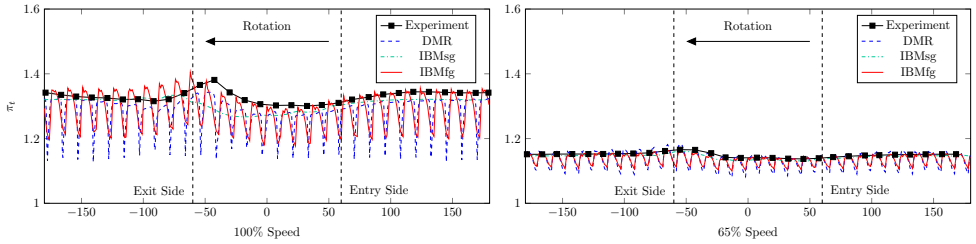

(b) Midspan, 50% blade height

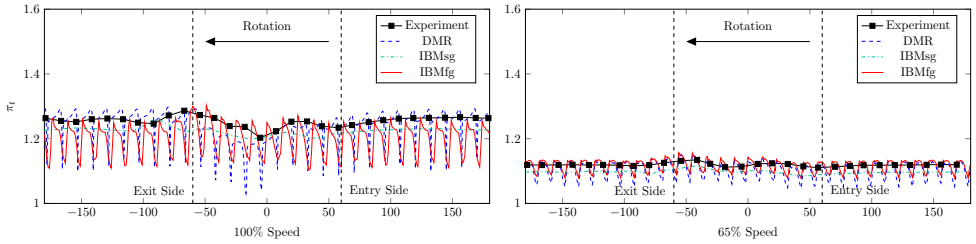

(c) Shroud, 90% blade height

Figure 5: Total pressure distribution at three radial locations at stator outlet:(a) Hub, (b) Midspan, (c) Shroud

blade leading edge. The pressure rises induced by the blade are generally well captured at all the blade passages. However, in Frame (a), near the casing the discrepancies becomes larger and the IBMfg case shows a much smoother distribution. This is perhaps because around the blade tip, the boundary layers are more sensitive to higher Ma. Since they are not well resolved, the velocity profiles and the static pressure may deviate further compared to the DMR case.

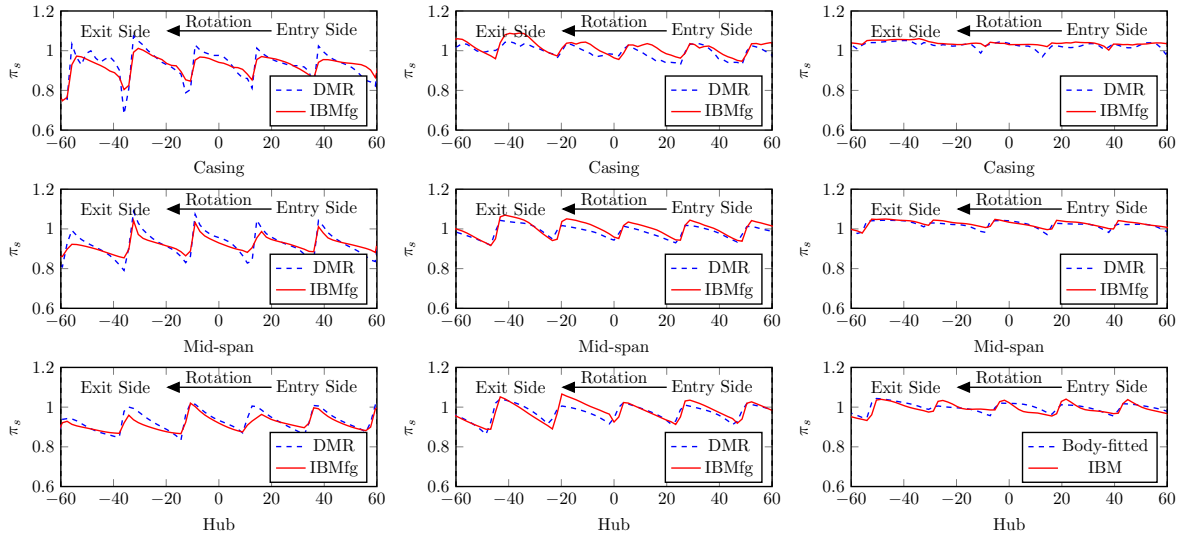

(a) Leading edge (b) Mid-chord (c) Trailing edge

Figure 6: Static pressure distribution at: (a) Leading edge, (b) Mid-chord, (c) Trailing edge

Similar trends can be also found at the blade mid-chord (Frame (b)), where the discrepancies becomes higher towards the casing as the velocity increases. Apart from this, at the casing within the separation region, the pressure rise area is much thicker than the DMR case, indicating that the development of boundary layer is underestimated. This can be improved by either advancing the loss model or refining the mesh around blade tip, depending on the requirement of flow details. At blade trailing edge (Frame (c)), the distributions of static pressure from both cases are generally matched. This demonstrates that the IBMfg can characterise the blade wakes accurately. However, it should be noted that near the casing the discrepancies for boundary layer development are still visible.

Hence, we may conclude that this IBMfg can provide a proper pressure intermittency for most part of the blade. However, special treatments may be needed to improve its performance near the tip clearance. This may include refining the mesh in this area or implementing some wall models.

CONCLUSIONS

The present research proposed a IBM with filtered geometry to investigation fan-intake interaction. This filtering process is based on a distribution function, via which the spatial and temporal features of rotational blades can be captured. This method can achieve similar performance compared to the conventional mesh-resolved geometry. It does not apply sliding planes across moving and static coordinates, does not need efforts to generate body-fitted mesh, and hence can maintain very low computational costs. To demonstrate its performance, the method is applied to the URANS simulation for a full-annulus rotor case. The results are compared against the experiment, the DMR case (URANS) and the IBMsg case (RANS).

The results demonstrate that the IBMfg is able to capture the main flow features for the full-annulus case. The distribution of static pressure and Ma are well represented. The total pressure distributions in both axial and radial locations are quantitatively compared. Both the general trends in the distortion region and downstream blade wakes are well reproduced. Within blade passages, although the boundary layer cannot be well resolved, the difference between pressure and suction surfaces are approximated successfully. This indicates that the pressure wave can be accurately generated.

The research shows that the IBMfg can be a very promising tool for the high-fidelity simulation in industry. For example, when investigating the acoustical influence of fan on the upstream with LES, one can apply the IBMfg to fan blades. This can significantly reduce the total mesh size and hence the eddy resolving method could be possible. However, there are still some drawbacks that need to deal with. Due to the limitation of loss models, this method may have problems for non-peaking efficiency points. This is because when the inlet massflow rate is either too high or too low, and the separation at blade trailing edge can be significant. Hence, the proposed parallel force in IBMfg cannot deviate the flow in the normal direction and thus the relevant distribution may be not accurate. In the future, this problem could be tackled by adding a deviation model calibrated by the data from efficiency map.

ACKNOWLEDGEMENT

The work is funded by the China Scholarship Council No. 201506020121. The computing time on the UK national high-performance computing service ARCHER is provided via the UK Turbulence Consortium in the framework of the EPSRC grant EP/L000261/1. The use of the UK ARCHER computational facility is also granted by the EPSRC Leadership project "Coupled, multi-scale modelling of modern installed aeroengine aeroacoustics". The code for this project is provided by the Rolls-Royce plc. All the funding and technical support from these organizations are gratefully appreciated.

References

Basdevant, C. and Sadourny, R. (1984). Numerical solution of incompressible flow: the mask method, *Lab di Meteorologie Dynamique, Ecole Normale Superieure, Paris (unpublished)* .

Bitter, M., Wartzek, F., Übelacker, S., Schiffer, H.-P. K. and J, C. (2015). Characterization of a distorted transonic compressor flow using dual-luminophore pressure-sensitive paint, *10th Pacific Symposium on Flow Visualization and Image Processing (PSFVIP-10), fedOA (Federico II Open Archive), Naples, Italy*.

Cao, T., Hield, P. and Tucker, P. G. (2016). Hierarchical immersed boundary method with smeared geometry, *54th AIAA Aerospace Sciences Meeting*, Vol. 33, p. 2130.

Defoe, J. J. and Spakovszky, Z. S. (2013). Effects of boundary-layer ingestion on the aero-acoustics of transonic fan rotors, *Journal of Turbomachinery* **135**(5): 051013.

Defoe, J., Narkaj, A. and Spakovszky, Z. (2009). A novel mpt noise prediction methodology for highly-integrated propulsion systems with inlet flow distortion.

Fadlun, E., Verzicco, R., Orlandi, P. and Mohd-Yusof, J. (2000). Combined immersed-boundary finite-difference methods for three-dimensional complex flow simulations, *Journal of computational physics* **161**(1): 35–60.

Goldstein, D., Handler, R. and Sirovich, L. (1993). Modeling a no-slip flow boundary with an external force field, *Journal of Computational Physics* **105**(2): 354–366.

Haase, W., Braza, M. and Revell, A. (2009). *DESider–A European Effort on Hybrid RANS-LES Modelling: Results of the European-Union Funded Project, 2004-2007*, Vol. 103, Springer Science & Business Media, Dordrecht.

Iaccarino, G. and Verzicco, R. (2003). Immersed boundary technique for turbulent flow simulations, *Applied Mechanics Reviews* **56**(3): 331–347.

Liu, Y., Lu, L., Fang, L. and Gao, F. (2011). Modification of spalart–allmaras model with consideration of turbulence energy backscatter using velocity helicity, *Physics Letters A* **375**(24): 2377–2381.

Liu, Y., Yan, H., Liu, Y., Lu, L. and Li, Q. (2016). Numerical study of corner separation in a linear compressor cascade using various turbulence models, *Chinese Journal of Aeronautics* **29**(3): 639–652.

Liu, Y., Yan, H., Lu, L. and Li, Q. (2017). Investigation of vortical structures and turbulence characteristics in corner separation in a linear compressor cascade using ddes, *Journal of Fluids Engineering* **139**(2): 021107.

Liu, Y., Yu, X. and Liu, B. (2008). Turbulence models assessment for large-scale tip vortices in an axial compressor rotor, *Journal of Propulsion and Power* **24**(1): 15–25.

Mittal, R. and Iaccarino, G. (2005). Immersed boundary methods, *Annu. Rev. Fluid Mech.* **37**: 239–261.

Mohd-Yusof, J. (1997). Combined immersed boudaries/b-splines methods for simulations in complex geometries.

Peskin, C. S. (2002). The immersed boundary method, *Acta numerica* **11**: 479–517.

Sirovich, L. (1967). Initial and boundary value problems in dissipative gas dynamics, *The Physics of Fluids* **10**(1): 24–34.

Spalart, P. R. (2000). Strategies for turbulence modelling and simulations, *International Journal of Heat and Fluid Flow* **21**(3): 252–263.

Tang, Y., Liu, Y. and Lu, L. (2018). Solidity effect on corner separation and its control in a high-speed low aspect ratio compressor cascade, *International Journal of Mechanical Sciences* **142**: 304–321.

Wartzek, F., Brandstetter, C., Holzinger, F. and Schiffer, H. (2015). Response of a transonic compressor to a massive inlet distortion, *European Turbomachinery Conference, Madrid, Spain, Mar*, pp. 23–27.

Wartzek, F., Holzinger, F., Brandstetter, C. and Schiffer, H.-P. (2016). Realistic inlet distortion patterns interacting with a transonic compressor stage, *Advances in Simulation of Wing and Nacelle Stall*, Springer, Cham, pp. 285–302.

Watson, R., Cui, J., Ma, Y. and Hield, P. (2017). Improved hierarchical modelling for aerodynamically coupled systems, *ASME Turbo Expo 2017: Turbine Technical Conference and Exposition*, American Society of Mechanical Engineers.